Published in final edited form as:
Plasmonics. 2008 March 1; 3(1): 3–11. doi:10.1007/s11468-007-9047-6.

Fluorescence Quenching of CdTe Nanocrystals by Bound Gold Nanoparticles in Aqueous Solution

Jian Zhang, **Ramachandram Badugu**, and **Joseph R. Lakowicz**
Center for Fluorescence Spectroscopy, Department of Biochemistry and Molecular Biology, University of Maryland School of Medicine, 725 West Lombard Street, Baltimore, MD 21201, USA

Abstract

Water-soluble gold nanoparticles with an average diameter of 5 nm were prepared with carboxylic acid terminated thiol ligands. These ligands contain zero to eight methylene moieties. CdTe nanocrystals with an average diameter of 5 nm were synthesized with aminoethanethiol capping. These nanocrystals displayed characteristic absorption and emission spectra of quantum dots. The amine terminated CdTe nanocrystals and carboxylic-acid-terminated gold nanoparticles were conjugated in aqueous solution at pH 5.0 by electrostatic interaction, and the conjugation was monitored with fluorescence spectroscopy. The CdTe nanocrystals were significantly quenched upon binding with gold nanoparticles. The quenching efficiency was affected by both the concentration of gold nanoparticles in the complex and the length of spacer between the CdTe nanocrystal and Au nanoparticle. The observed quenching was explained using Förster resonance energy transfer (FRET) mechanism, and the Förster distance was estimated to be 3.8 nm between the donor-acceptor pair.

Keywords

CdTe nanocrystal; Gold nanoparticle; Fluorescence quenching; Electrostatic interaction; Energy transfer

Introduction

Because of chemical stability, well-developed surface chemistry, and unique optical properties, the noble metallic nanoparticles are becoming attractive in chemistry and biology applications [1-9]. Occurrence of fluorescence near metallic nanoparticles is a complicated near field interaction. Considerable theoretical and experimental efforts are being made to understand the influence of the metal substrate on the emission spectral properties of fluorophores [10, 11]. Over several years, we are trying to understand the interactions of fluorophores with the metallic surfaces or metal nanoparticles [7,12-23]. It is known that a fluorophore near a metal film/metallic particle shows a varied luminescence depending on the distance from the metal surface [24,25]. A short distance from the metal nanoparticles, particularly the gold particles, can bring up efficient quenchers [26,27]. Thus, the metal particles can be applied in designing the biological and chemical beacon measurements.

Most quenching studies involving fluorophores and metal nanoparticles focus on organic fluorophores [1,2,26,27]. However, the organic fluorophores show obvious photobleaching during the experiments [28,29]. Semiconductor nanoparticles (commonly known as QDots)

lakowicz@cfs.umbi.umd.edu.

show enormous photostability over regular organic fluorophores [30-34]. They also display size-tunable absorption and emission properties due to quantum size effect. The luminescent QDots have gained much interest in various research fields, including in vivo biological imaging, optoelectronics industry, and therapeutics, etc. [35-37]. In this paper, we investigated the fluorescence quenching of CdTe nanocrystals by gold nanoparticles when binding them as complexes by electrostatic interactions of oppositely charged surface ligands. The quenching efficiency of the fluorophore by the metal particle depends on many factors [38-40] in which the spacer that are used to separate the fluorophore from the metal particle may influence the overall quenching efficiency. Firstly, the change in spacer length may induce conformational changes. Secondly, the change of linker length and composition can influence the magnitude of through-bond coupling between the fluorophore and metal core. Thirdly, the quenching due to energy and electron transfer is well known to depend strongly on the distance/spacer length.

Herein, we synthesized the CdTe nanocrystals using 2-mercaptoethylamine as surface protecting ligand [41,42]. These CdTe nanocrystals (having average core diameter of ~5 nm and being coated by terminated amine groups) were conjugated with the gold nanoparticles (having average core diameter ~5 nm and being coated by carboxylic acid moieties; Scheme 1; [43,44]) In buffer solution at pH 5.0, the surfaces of metal nanoparticles were negatively charged due to the deprotonation of carboxylic acid ligands; while the surfaces of the CdTe nanocrystals were positively charged by the protonated amine ligands. Hence, the metal particles and CdTe nanocrystals were conjugated strongly by electrostatic interactions (Scheme 2). This conjugation procedure was monitored using fluorescence spectroscopy. Upon mixing with the metal particles, the fluorescence spectra of CdTe nanocrystals showed a steady time-dependent intensity decrease, which relied on both the concentration of metal particles and spacer lengths between the CdTe nanocrystals and gold nanoparticles.

Experimental section

All the reagents and spectroscopic grade solvents were used as received from Fisher or Aldrich. Nanopure water (>18.0 M cm), purified using Millipore Milli-Q gradient system, was used in all experiments. The ligand (2-mercapto-propionylamino) acetic acid 2,5-dioxo-pyrrolidin-1-ylester was synthesized as described in the previous report [45].

Preparation of CdTe nanocrystals

The synthesis of CdTe nanocrystals was performed using a modified Weller procedure described below [41,42]. Briefly, a solution of 1.970 g $Cd(ClO_4)_2\,6H_2O$ (4.70 mmol) and 0.900 g stabilizing ligand, mercaptoethylamine, (11.54 mmol) was placed in 250 mL MilliQ-water. The solution pH was adjusted to 6.0 by adding a few drops of diluted HCl, and then the solution was continuously stirred for 30 min at room temperature with nitrogen purging to eliminate dissolved oxygen. The source of tellurium (NaHTe) was prepared separately, which involved the reduction of metallic tellurium powder (0.383 g, 3 mmol) suspended in 10 mL MilliQ-water with sodium borohydride (0.227 g, 6 mmol in 5 mL water) at 0-5°C. In an about 30 min, the suspended tellurium powder completely dissolves in water, and the color of solution was changed to pinkish. Under vigorous stirring, the obtained NaHTe solution was injected slowly into the solution of $Cd(ClO_4)_2\,6H_2O$ containing mercaptoethylamine at room temperature. The reaction mixture was refluxed for 2 h and then cooled down to room temperature. The resulting red color solution was purified by centrifugation. The residue was redispersed in water and centrifuged further for complete elimination of unreacted Cd^{2+} ions. The pH of the final solution was adjusted to 5.0 using 1.0 mM $HClO_4$ solution. We noticed very similar fluorescence quenching behavior, when we used both pure and as prepared CdTe nanocrystals in the present experiments. This might be due to either insignificant amount of Cd^{2+} ions in

the CdTe solutions or relatively much weaker binding affinity of Cd^{2+} ions over the CdTe nanocrystals with multiple positively charged ammonium cations with metal nanoparticles.

Preparation of monolayer-protected gold nanoparticles

Gold nanoparticles were prepared by a modified Brust method [43-46]. Briefly, a dilute two-phase water/toluene solution of $HAuCl_4$ was reduced with $NaBH_4$ in the presence of tetraoctylammonium bromide. After complete reduction, the supernatant toluene was separated from water. Subsequently, toluene was removed under vacuum, and the residual solid was washed thoroughly with methanol. The ligands on Au particles (30 mg) were replaced by *N*-(2-mercaptopropionyl) glycine (tiopronin) or (2-mercaptopropionylamino) acetic acid 2,5-dioxo-pyrrolidin-1-ylester (10 mg) in 25 mL toluene/methanol mixed solvent (*v*/*v*=1:1). The solution was stirred at room temperature for 4 h to form a thiolate monolayer. The solvent was removed under vacuum, and the residue was washed with methanol. A black solid was collected on a 0.2-mm membrane filter. The succinimidylated Au particles (10 mg) and γ-amino alkyl carboxylic acid derivatives (5 mg) were co-dissolved in 10 mL methanol and stirred for 2 h at room temperature. The solvent was removed under vacuum, and the residual solid was washed with methanol. The final condensation products were dissolved in 10 mL water and dialyzed completely against water.

Preparation of the CdTe-Au complex

The monolayer-protected gold nanoparticles were dissolved in water, and the pH was adjusted to 5.0 using 1 mN $HClO_4$ solution. The solution of CdTe nanocrystals was added to the above solution of Au nanoparticles in a required mole ratio. The fluorescence spectral changes were monitored immediately to investigate the binding kinetics of the CdTe nanocrystals with gold nanoparticles.

Spectral measurements

Absorption and fluorescence spectra of the samples were recorded on a Hewlett Packard 8453 spectrophotometer and Cary Eclipse Fluorescence Spectrophotometer, respectively. Transmission electron micrographs (TEM) were taken with a side-entry Philips electron microscope at 120 keV. Samples were cast from water solutions onto standard carbon-coated (200-300 Å) Formvar films on copper grids (200 mesh) by placing a droplet of a 1 mg/mL aqueous sample solution on grids. The size distribution of metal core was analyzed with Scion Image Beta Release 2 counting at least 200 particles. Time-resolved intensity decays were recorded using a PicoQuant Fluotime 100 time-correlated single-photon counting (TCSPC) fluorescence lifetime spectrometer. The excitation at ~470 nm was obtained using a pulsed laser diode (PicoQuant PDL800-B) with 20 MHz repetition rate. The Instrument Response Function (IRF) is about 300 ps. The excitation was vertically polarized, and the emission was recorded through a polarizer oriented at 54.7° from the vertical position. A longpass filter at 530 nm (Chroma) was used in the collection path to eliminate the scattered excitation light.

Data analysis

The fluorescence intensity decays were analyzed in terms of the multi-exponential model as the sum of individual single exponential decays: [29]

$$I(t) = \sum_{i=1}^{n} \alpha_i \exp(-t/\tau_i) \quad (1)$$

In this expression, τ_i is the decay time and α_i is the amplitude and $\sum_i \alpha_i = 1.0$. The fractional contribution of each component to the steady-state intensity is described by:

$$f_i = \frac{\alpha_i \tau_i}{\sum_j \alpha_j \tau_j} \tag{2}$$

The average lifetime is represented by:

$$\bar{\tau} = \sum_i f_i \tau_i \tag{3}$$

and the amplitude-weighted lifetime is given by:

$$<\tau> = \sum_i \alpha i \tau i \tag{4}$$

The values of α_i and τ_i were determined using the PicoQuant Fluofit 3.3 software with the deconvolution of instrument response function and nonlinear least squares fitting. The goodness-of-fit was determined by the χ^2 value.

Results and discussion

Figure 1 presents the TEM images of individual CdTe nanocrystals, gold nanoparticles, and CdTe-Au complex, respectively. Although the images of CdTe nanoparticles (Fig. 1a) were not that clear (Fig. 1b), their average core size could be approximately estimated to be ~5 nm. These amine-terminated CdTe nanocrystals showed a stable dispersion in water. The nanocrystals displayed a characteristic absorption spectrum as observed with the other QDots with the absorption maximum at 522 nm (Fig. 2) and an emission maximum at 535 nm in aqueous solution when they were excited at 450 nm. No noticeable change in the emission wavelength and intensity was observed when the CdTe nanocrystals were continuously exposed to the excitation light for 2 h in solution, indicating they were photostable under the current experiment conditions. The extinction coefficient of CdTe nanocrystal at 522 nm was estimated to be 3.2×10^5 cm^{-1} M^{-1}. The concentration of CdTe nanocrystal in buffer solution was 5.0×10^{-7} M in all experiments.

Tetraoctylammonium-coated gold nanoparticles were prepared using a modified Brust method. Their TEM images showed an average core diameter of 5 nm (Fig. 1b), close to the size of CdTe nanocrystals. The size of gold nanoparticles was not altered significantly after displacing the tetraoctylammonium ligands with tiopronin or (2-mercapto-propionylamino) acetic acid 2,5-dioxopyrrolidin-1-ylester, indicating the insignificant core disruption during the exchange reaction. However, we noticed about 10 nm shift of absorbance wavelength (from 520 nm to 530 nm) with the ligand exchange, implying that the metal plasmon absorbance was sensitive to the monolayer composition and surrounding environment on the metal cores (Fig. 2; [47-49]). Although the TEM images of gold particles did not alter significantly before and after ligand exchange, these metal particles displayed an obvious ligand-dependent solubility: the tetraoctylammonium-coated gold particles were dissolved in toluene but poor in alcohol; while the tiopronin-coated metal particles showed a good solubility in water but also poor in alcohol. Different from them, the succinimidylated Au particles were dissolved well in alcohol but slightly in water. The extinction coefficient of tiopronin-coated gold particle at 530 nm was

estimated to be 4.5×10^5 cm^{-1} M^{-1}. No significant emission was observed for any gold nanoparticles in this study.

The succinimidylated Au particles reacted with γ-amino alkyl carboxylic acids to generate the longer ligands having carboxylic acid terminal. The number of methylene moieties for the γ-amino alkyl carboxylic acids were 3, 6, and 8, respectively. The γ-amino alkyl carboxylic acid with a longer methylene moiety was found to have a poor solubility in a convenient organic solvent that could simultaneously dissolve the gold nanoparticles, so the derivatives utilized in this study had a maximal methylene moiety of eight. All carboxylated metal nanoparticles displayed good solubility in water at pH 5.0.

The CdTe nanocrystals were mixed with the gold nanoparticles in buffer solution at pH 5.0, at which the carboxylic acid moieties on the gold nanoparticles were deprotonated. Hence, the particle surfaces were negatively charged. Contrarily, the amine moieties on the CdTe nanocrystals were protonated, giving rise to positively charged CdTe nanocrystal surfaces. Subsequently, the positive-charged CdTe nanocrystals and negative-charged gold nanoparticles were expected to form the complexes in solution due to electrostatic interactions. Because both the CdTe and gold nanoparticles were multiple-functionalized, the conjugation resulted in an aggregate of them. Accordingly, it was quite convincing from the TEM image (Fig. 1c), on which the large compact 3-dimensional CdTe-Au complexes were observed clearly.

Because of significant and wide-range absorption spectral overlap of the CdTe nanocrystals and gold nanoparticles (Fig. 2), it was difficult to monitor the conjugation process using the absorption spectrum, but convenient using fluorescence spectra. Fluorescence from CdTe nanocrystals displayed a significant time-dependent quenching with the conjugation. The experiment result revealed that the quenching was reliant on both the concentration of gold nanoparticles and length of the linker between them (*vide infra*).

We first studied the concentration effect of gold nanoparticles on the kinetics of conjugation between them. The tiopronin-coated gold nanoparticle (i.e., shortest ligand) was used in this study. A significant fluorescence quenching from the CdTe nanocrystal was observed with the binding of metal nanoparticles: although the emission wavelength remained the same, but the intensity decreased (Fig. 3). The emission intensity at 535 nm for the samples with different mole ratios of gold/CdTe was plotted against the binding time (Fig. 4a) showing that the fluorescence was quenched very rapidly at the initial period, but became slow with time proceeding, and then reached a plateau at final. The fluorescence intensity dropped faster when the concentration of gold nanoparticle was high in solution. In the other words, a low molar ratio of the metal particle/CdTe nanocrystals resulted in a slower binding process, and the binding kinetics rapidly increased with the mole ratio of gold/CdTe nanoparticles. The quenching efficiency, estimated on the basis of the emission intensity, displayed a significant increase and reached to a steady state at the metal concentration of 50 nM (Fig. 4b). It means that most of the CdTe nanocrystals have been quenched at a molar ratio of metal particle/CdTe nanocrystal of 0.1 showing that the aggregates contain 10 CdTe nanocrystals per one gold nanoparticle.

We discussed the quenching of CdTe nanocrystals by the gold nanoparticles separated with the shortest ligand. However, the fluorescence quenching is a distance-dependent process [29]. In this study, we hence prepared the gold nanoparticles with varied linker lengths. Figure 5 shows the binding kinetics of Au/CdTe complex with different lengths of spacer. Control experiment, i.e., the CdTe nanocrystals in buffer solution without gold nanoparticles, showed almost no change in fluorescence intensity. On the other hand, the gold nanoparticles with the eight methylene carbons showed the weakest ability of fluorescence quenching. Fluorescence

quenching ability by the bound gold nanoparticles was noticed to increase with decreasing methylene carbon number from 8 to 0. Thus, we can say that the quenching efficiency decreases with increasing length of the spacer moiety (Fig. 5b).

The observed fluorescence quenching of CdTe nanocrystals by the metal particles is expressed by Förster energy transfer process [44], and the quenching rate constant by metal particle generally depends on the donor-acceptor (in the present case, CdTe nanocrystals and gold nanoparticles, respectively) distance as in Eq. 5,

$$k_{\mathrm{m}}=\frac{1}{\tau_{\mathrm{D}}}\left(\frac{R_{\mathrm{o}}}{r}\right)^{6} \tag{5}$$

where, τ_{D} is the lifetime of the donor in the absence of acceptor, R_{o} is the Förster distance, and r is the donor-to-acceptor distance. It is impossible to obtain R_{o} directly from Fig. 6b, but we can infer it according to a forward extension of curve that was near 12 methylene moieties. The spacer length can be estimated by calculating van der Waals contact distances and by assuming a zigzag conformation for each moiety. So R_{o} is estimated to be 3.8 nm, which is in accordance with the regular values of Förster distance for the organic donor-acceptor pair [29].

The fluorescence intensity shows multiexponential decay kinetics, which is due to the polydisperse size-distribution of the QDots in solution. However, we can obtain reasonably good fit to the curves of intensity decays in this case. The lifetime data of CdTe nanocrystals and CdTe-Au complexes are depicted in Table 1. CdTe nanocrystals show an average lifetime of 22 ns in the absence of Au nanoparticles, and the lifetime decreased by 56% with the binding of gold nanoparticles with the shortest linker space. Interestingly, the CdTe nanoparticles showed a consistent increase in the lifetimes with the tendency of the spacer length (12.2 to 16.6 ns from zero to eight methylene moiety). The quenching rate constant k_{m} that is estimated using the lifetime of CdTe nanocrystals in the absence of metal nanoparticle is plotted against the number of methylene carbons (Fig. 6a), showing that the rate constant decreases with increasing the spacer length.

The quenching efficiency is verified to depend on the distance between the CdTe nanocrystals and metal particle (Fig. 6b). According to Equation 5, the quenching efficiency (E) can be expressed as Eq. 6.

$$E=\frac{R_{\mathrm{o}}^{6}}{R_{\mathrm{o}}^{6}+r^{6}} \tag{6}$$

The estimated E values are plotted against r/R_{o} (Fig. 6b), showing a typical decrease of efficiency with the distance. Because of the limitation of spacer lengths we used in this study, we can only give the first half of the sigmoidal quenching efficiency curve.

Conclusions

The amino-terminated thiol-coated CdTe nanocrystals were synthesized in aqueous solution and had an average core diameter of 5 nm. The water-soluble gold nanoparticles having similar average core diameters of 5 nm were prepared by a modified Brust method. The surfaces of metal particles were coated by the carboxylic acid-terminated thiolate ligands whose length is modulated by the condensation of γ-aminoalkylcarboxylic acids. In water solution at pH 5.0, the carboxylic-acid-terminated metal particles and amine-terminated CdTe nanocrystals are

attached together to form complexes because of favorable electrostatic interactions. The static binding is revealed by TEM images, showing the formation of aggregates. Subsequently, the metal nanoparticles were verified to work as efficient quenchers during the binding with the CdTe nanocrystals. The binding kinetics showed that the CdTe nanocrystals were quenched more rapidly with increasing concentration of metal particle in the complex. The quenching efficiency was found to be affected by the spacer length of linker between the QDot and metal particle. Using the Förster energy transfer model, the quenching rate constants were estimated depending on the spacer lengths. The Förster distance was 3.8 nm. This result shows that the QDot-metal particle complex can be utilized to set up a donor-acceptor pair for the quenching via energy transfer in biological and chemical sensing.

Acknowledgments

This research was supported by a grant from NIH, HG-02655, EB-00682, and NCRR, RR-08119.

References

1. Thomas KG, Kamat PV. Chromophore-functionalized gold nanoparticles. Acc Chem Res 2003;36:888–898. [PubMed: 14674780]
2. Kamat PV. Photophysical, photochemical and photocatalytic aspects of metal nanoparticles. J Phys Chem B 2002;106:7729–7744.
3. Emory SR, Haskins WE, Nie S. Direct observation of size-dependent optical enhancement in single metal nanoparticles. J Am Chem Soc 1998;120:8009.
4. Goodrich GP, Helfrich MR, Overberg JJ, Keating CD. Effect of macromolecular crowding on DNA: Au nanoparticle bioconjugate assembly. Langmuir 2004;20:10246–10251. [PubMed: 15518520]
5. Josephson L, Kircher MF, Mahmood U, Tang Y, Weissleder R. Near-infrared fluorescent nanoparticles as combined MR/optical imaging probes. Bioconjugate Chem 2002;13:554–560.
6. Yu F, Persson B, Lofas S, Knoll W. Surface plasmon fluorescence immunoassay of free Prostate-specific antigen in human plasma at the femtomolar level. Anal Chem 2004;76:6765–6770. [PubMed: 15538801]
7. Lakowicz JR. Radiative decay engineering 5: metal-enhanced fluorescence and plasmon emission. Anal Biochem 2005;337:171–194. [PubMed: 15691498]
8. Rosi NL, Mirkin CA. Nanostructures in biodiagnostics. Chem Rev 2005;105:1547–1562. [PubMed: 15826019]
9. Love JC, Estroff LA, Kriebel JK, Nuzzo RG, Whitesides GM. Self-assembled monolayers of thiolates on metals as a form of nanotechnology. Chem Rev 2005;105:1103–1170. [PubMed: 15826011]
10. Adams A, Rendell RW, Garnett RW, Hansma PK, Metiu H. Effect of metal-film thickness on surface-atom coupling. Optics Commun 1980;34:417–410.
11. Aussenegg FR, Leitner A, Lippitsch ME, Reinisch H, Riegler M. Novel aspects of fluorescence lifetime for molecules positioned close to metal surfaces. Surf Sci 1987;139:935–945.
12. Lakowicz JR, Shen Y, D'Auria S, Malicka J, Fang J, Grcyzynski Z, Gryczynski I. Radiative decay engineering. 2. effects of silver island films on fluorescence intensity, lifetimes, and resonance energy transfer. Anal Biochem 2002;301:261–277. [PubMed: 11814297]
13. Lakowicz JR. Radiative decay engineering 3. Surface plasmon-coupled directional emission. Anal Biochem 2004;324:153–169. [PubMed: 14690679]
14. Lakowicz JR, Shen Y, Grcyzynski Z, D'Auria S, Gryczynski I. Intrinsic fluorescence from DNA can be enhanced by metallic particles. Biochem Biophys Res Commun 2001;286:875–879. [PubMed: 11527380]
15. Aslan K, Gryczynski I, Malicka J, Matveeva E, Lakowicz JR, Geddes CD. Metal-enhanced fluorescence: an emerging tool in biotechnology. Curr Opin Biotechnol 2005;16:55–62. [PubMed: 15722016]
16. Aslan K, Lakowicz JR, Geddes CD. Plasmon light scattering in biology and medicine: new sensing approaches, visions and perspectives. Curr Opin Chem Biol 2005;9:538–544. [PubMed: 16129649]

17. Malicka J, Gryczynski I, Lakowicz JR. DNA Hybridization Assays Using Metal-enhanced Fluorescence. Biochem Biophys Res Commun 2003;306:213–218. [PubMed: 12788090]
18. Lakowicz JR, Malicka J, D'Auria S, Gryczynski I. Release of the self-quenching of fluorescence near silver metallic surfaces. Anal Biochem 2003;320:13–20. [PubMed: 12895465]
19. Aslan K, Lakowicz JR, Geddes CD. Metal-enhanced fluorescence using anisotropic silver nanostructures: critical progress to date. Anal Bioanal Chem 2005;382:926–933. [PubMed: 15937664]
20. Geddes, CD.; Aslan, K.; Malicka, J.; Gryczynski, I.; Lakowicz, JR. In annual reviews in fluorescence. Geddes, CD.; Lakowicz, JR., editors. Kluwer/Plenum; New York: 2004.
21. Geddes, CD.; Aslan, K.; Malicka, J.; Gryczynski, I.; Lakowicz, JR. Topics in fluorescence spectroscopy. Geddes, CD.; Lakowicz, JR., editors. Kluwer/Plenum; New York: 2005.
22. Weitz DA, Garoff S, Hanson CD, Gramila TJ, Gersten JI. Fluorescent lifetimes of molecules on silver-island films. Opt Lett 1982;7:89–91. [PubMed: 19710833]
23. Wokaun A, Lutz H-P, King AP, Wild UP, Ernst RR. Energy transfer in surface enhanced luminescence. J Chem Phys 1983;79:509–514.
24. Drexhage, KH. Progress in optics XII. Wolf, E., editor. North Holland; Amsterdam: 1974.
25. Lakowicz JR. Radiative decay engineering: biophysical and biomedical applications. Anal Biochem 2001;298:1–24. [PubMed: 11673890]
26. Aguila A, Murray RW. Monolayer-protected clusters with fluorescent dansyl ligands. Langmuir 2000;16:5949–5954.
27. Zhang J, Whitesell JK, Fox MA. Photophysical behavior of variously sized colloidal gold clusters capped with monolayers of an alkylstilbenethiolate. J Phys Chem B 2003;107:6051–6055.
28. Lakowicz, JR. Emerging biomedical application of time-resolved florescence spectroscopy, topic in fluorescence spectroscopy, vol (4), probe design and chemical sensing. Lakowicz, JR., editor. Plenum; New York: 1994.
29. Lakowicz, JR. Principles of fluorescence spectroscopy. Vol. 2nd edn.. Kluwer; New York: 1999.
30. Empedocles S, Bawendi M. Spectroscopy of single CdSe nanocrystallites. Acc Chem Res 1999;32:389.
31. Penner RM. Hybrid electrochemical/chemical synthesis of quantum dots. Acc Chem Res 2000;33:78–86. [PubMed: 10673315]
32. Gaponik N, Talapin DV, Rogach AL, Eychmuller A, Weller H. Efficient phase transfer of luminescent thiol-capped nanocrystals: from water to nonpolar organic solvents. Nano Lett 2002;2:803–806.
33. Kapitonov AM, Stupak AP, Gaponenko SV, Petrov EP, Rogach AL, Eychmuller A. Luminescence properties of thiol-stabilized CdTe nanocrystals. J Phys Chem B 1999;103:10109–101113.
34. Tsay JM, Pflughoefft M, Bentolila LA, Weiss S. Hybrid approach to the synthesis of highly luminescent CdTe/ZnS and CdHgTe/ZnS nanocrystals. J Am Chem Soc 2004;126:1926–1927. [PubMed: 14971912]
35. Dubertret B, Skourides P, Norris DJ, Noireaux V, Briovanlou AH, Libchaber A. In vivo imaging of quantum dots encapsulated in phospholipid micelles. Science 2002;298:1759–1762. [PubMed: 12459582]
36. Larson DR, Zipfel WR, Williams RM, Clark SW, Bruchez MP, Wise FW, Webb WW. Water-soluble quantum dots for multiphoton fluorescence imaging in vivo. Science 2003;300:1434–1436. [PubMed: 12775841]
37. Rogach AL, Harrison MT, Kershaw SV, Kornowski A, Burt MG, Eychmuller A, Weller H. Colloidally prepared CdHgTe and HgTe quantum dots with strong near-infrared luminescence. Phys Status Solidi B 2001;224:153–158.
38. Nordlander, P. In laser spectroscopy and photochemistry on metal surfaces, part I. Dai, H-L.; Ho, W., editors. World Science; Singapore: 1995.
39. Winkler JR, Gray HB. Electron transfer in rutheniummodified proteins. Chem Rev 1992;92:369–379.
40. Fox MA. Fundamentals in the design of molecular electronic devices: long-range charge carrier transport and electronic coupling. Acc Chem Res 1999;32:201–207.

41. Gaponik N, Talapin DV, Rogach AL, Hoppe K, Shevchenko EV, Kornowski A, Eychmüller A, Weller H. Thiol-capping of CdTe nanocrystals: an alternative to organometallic synthetic routes. J Phys Chem B 2002;106:7177–7165.

42. Rogach AL, Kornowski A, Gao M, Eychmüller A, Weller H. Synthesis and characterization of a size series of extremely small thiol-stabilized CdSe nanocrystals. J Phys Chem B 1999;103:3065–3069.

43. Huang T, Murray RW. Visible luminescence of watersoluble monolayer-protected gold clusters. J Phys Chem B 2001;105:12498.

44. Huang T, Murray RW. Quenching of [Ru(bpy)3]2+Fluorescence by binding to Au nanoparticles. Langmuir 2002;18:7077–7081.

45. Zhang J, Roll D, Geddes CD, Lakowicz JR. Aggregation of silver nanoparticle-dextran adducts with Concanavalin A and competitive complexation with glucose. J Phys Chem B 2004;108:12210.

46. Brust M, Walker M, Bethell D, Schiffrin DJ, Whyman R. Synthesis of thiol-derivatized gold nanoparticles in a 2-phase liquid-liquid system. J Chem Soc Chem Commun 1994;7:801–802.

47. Foss, CA.; Feldheim, DL. Metal nanoparticles. synthesis, characterization and applications. Marcel Dekker; New York: 2001.

48. Kreibig, U.; Vollmer, M. Optical properties of metal clusters. Springer; Berlin: 1995.

49. Hayat, MA., editor. Colloidal gold: principles, methods, and applications. Academic; San Diego: 1991.

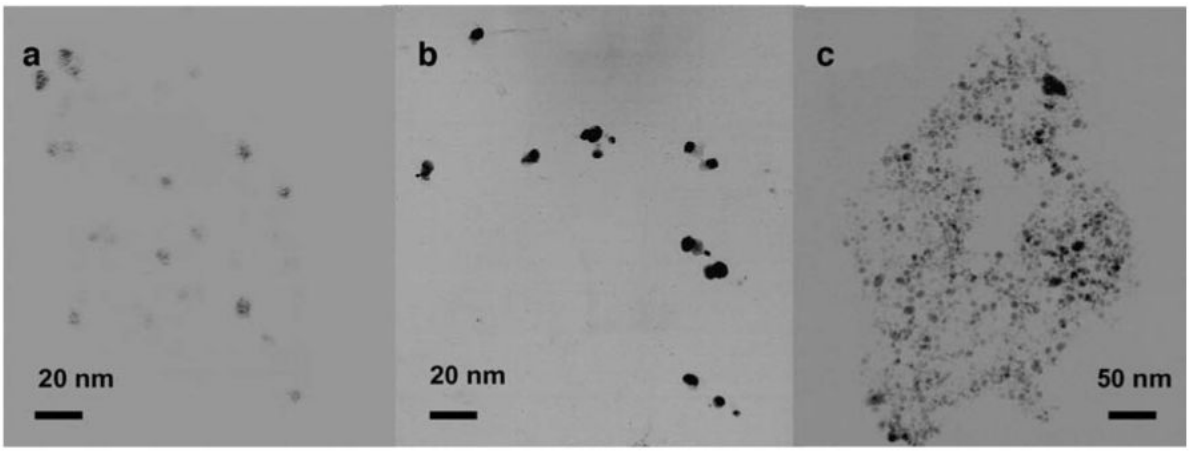

Fig. 1.
TEM images of individual **a** CdTe nanocrystals, **b** Au nanoparticles, and **c** corresponding complexes of CdTe nanocrystals and Au nanoparticles

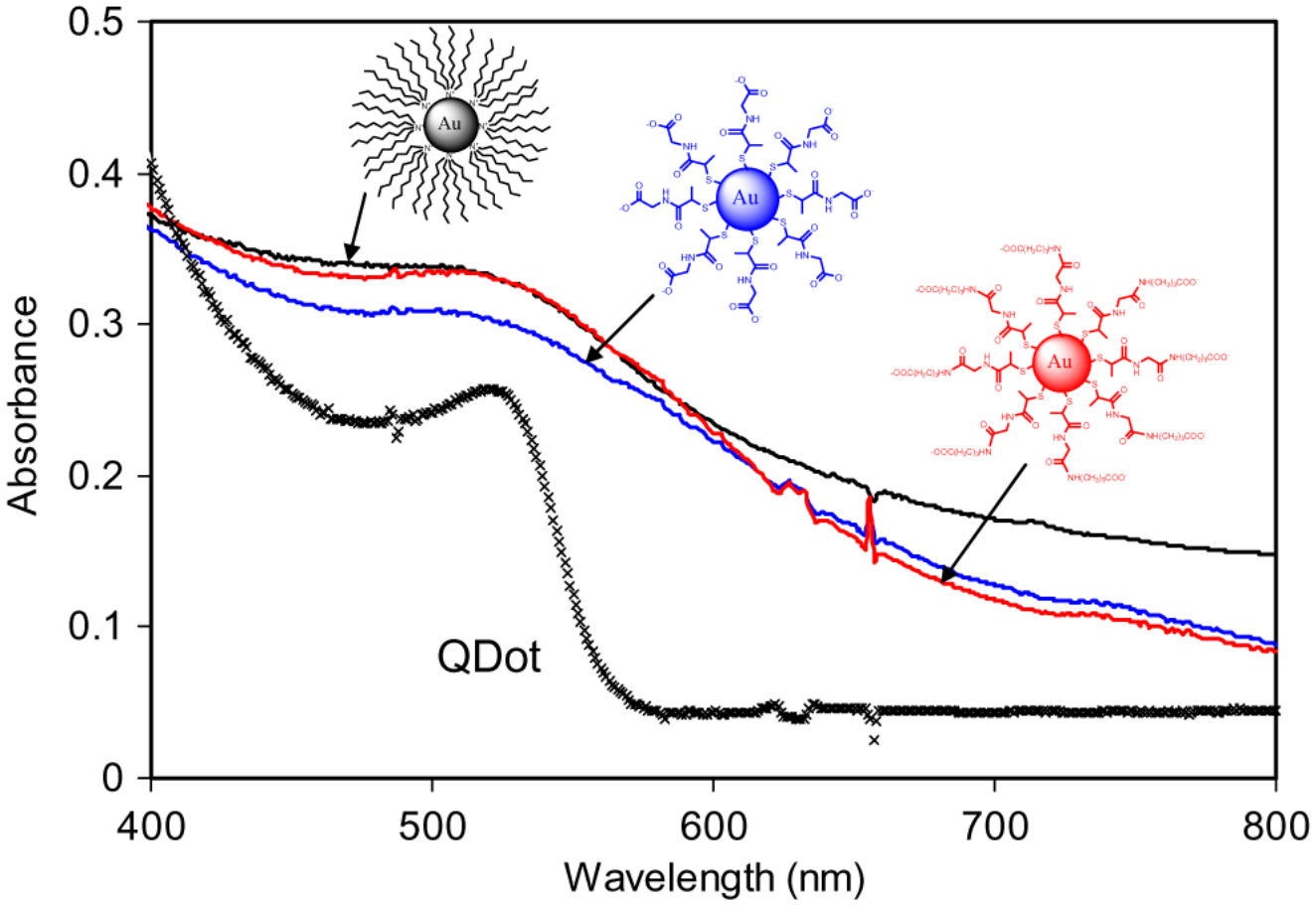

Fig. 2.
Absorbance spectra of tetraoctylammonium-coated gold nanoparticles, tiopronin-coated gold nano nanoparticle, and gold nanoparticles capped with longer linker ligands, and QDot in aqueous solution

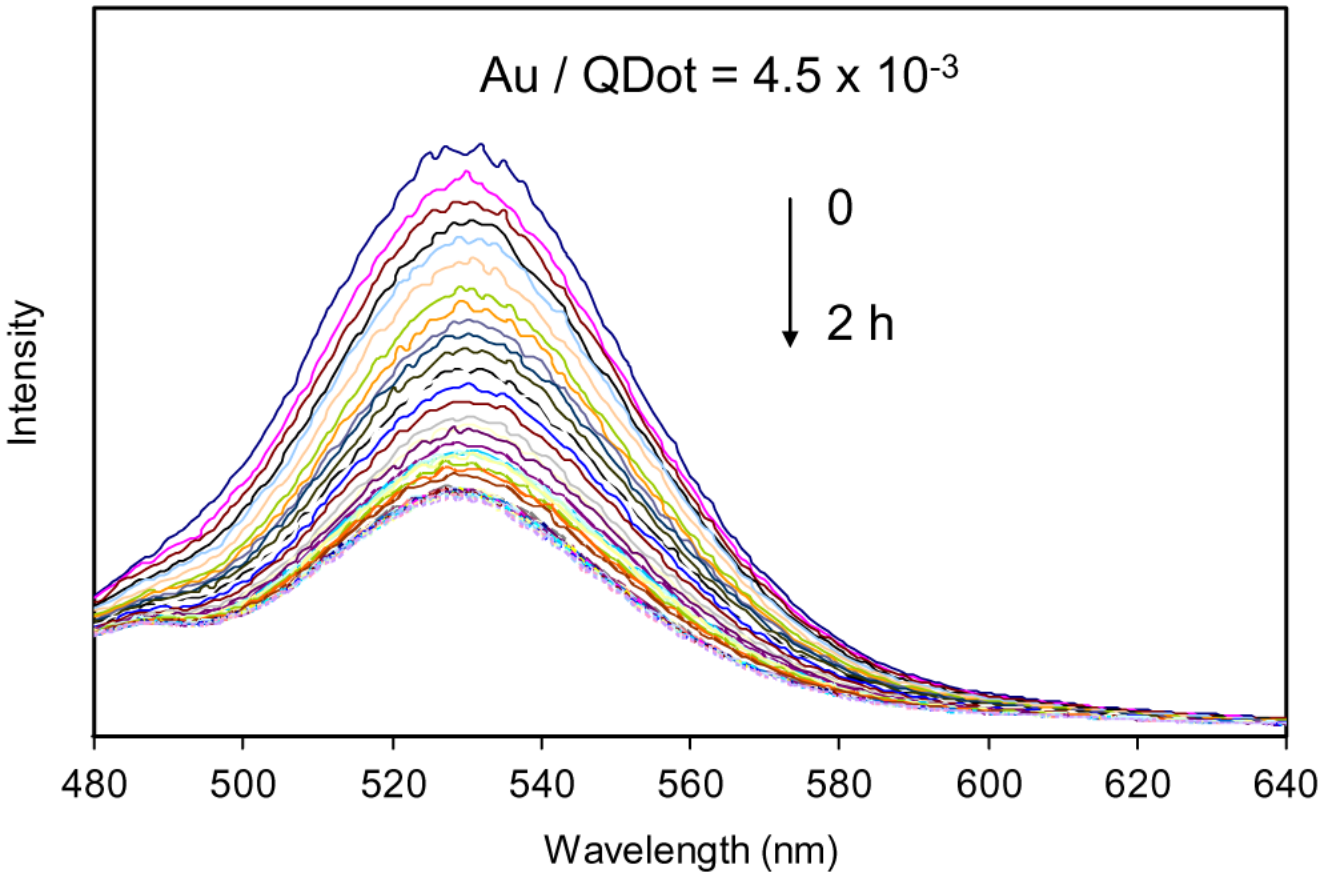

Fig. 3.
Fluorescence emission spectra of CdTe-tiopronin-protected gold nanoparticles with time (molar ratio of Au particle/QDot=4.5×10^{-3}). λ_{ex}=450 nm. The concentration of CdTe nanocrystal was 5.0×10^{-7} M in solution

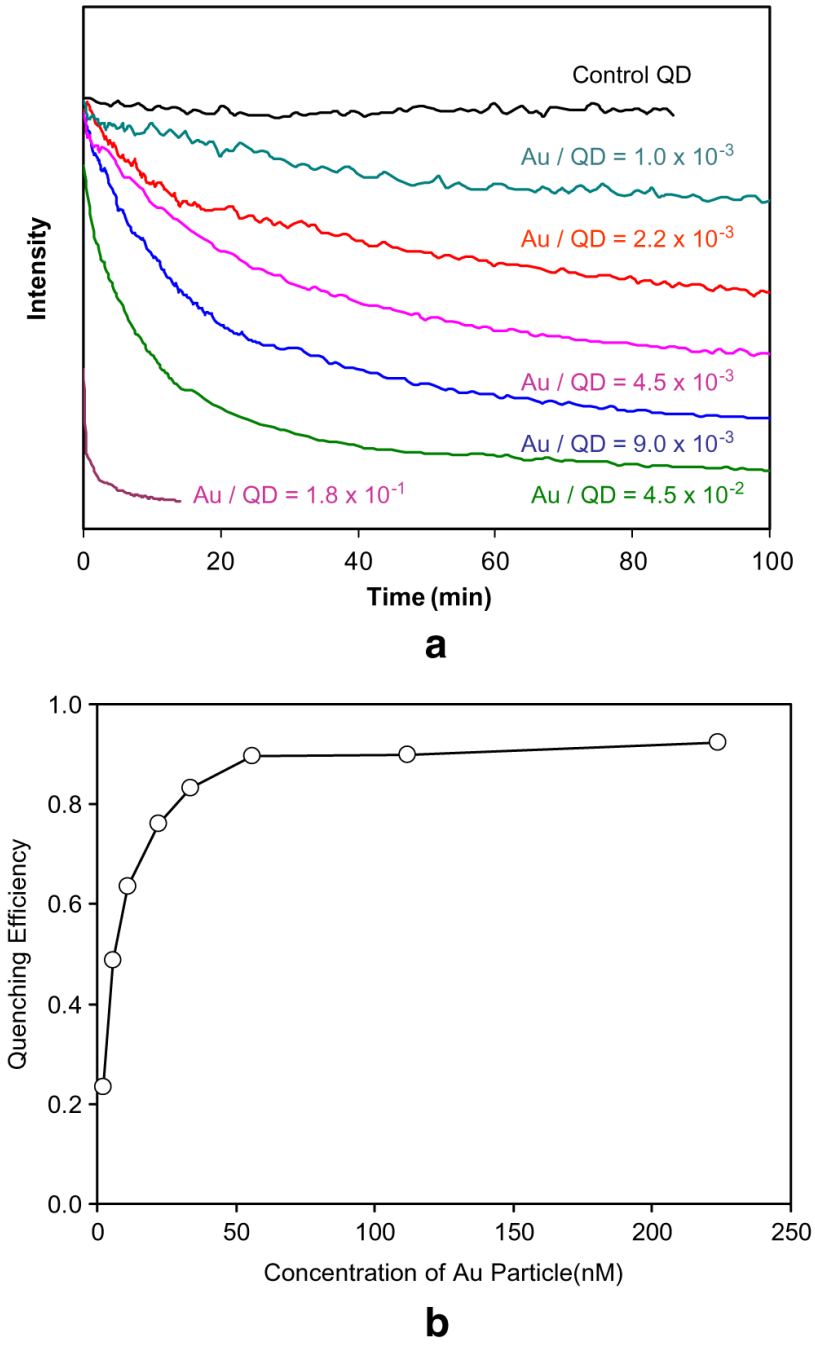

Fig. 4.

aChange in CdTe fluorescence intensity at 535 nm during the binding time with different molar ratios of Au nanoparticle/CdTe nanocrystals in solution and **b** effect of gold nanoparticles concentration on the CdTe fluorescence quenching efficiency. Fluorescence intensity at 535 nm after complete binding [plateau region from figure (**a**)] was used in this plot. The gold nanoparticles used herein are protected with shortest spacer, tiopronin (methylene number = 0). The concentration of CdTe nanocrystal was 5.0×10^{-7} M in solution

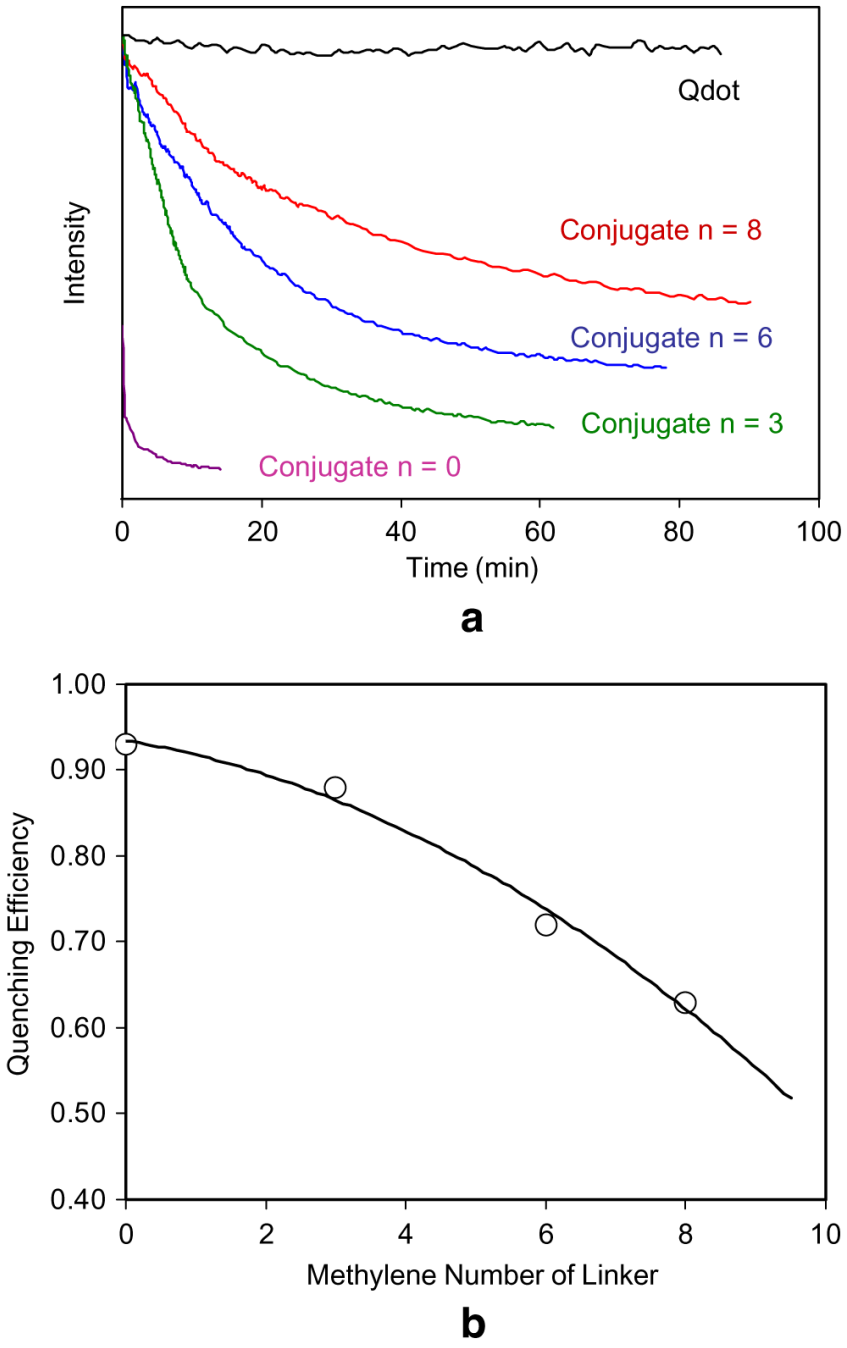

Fig. 5.

a Change in fluorescence intensity at 535 nm during binding time for the samples with different methylene number as the spacers between the metal particle and QDot in solution. **b** Effect of spacer length on the fluorescence quenching efficiency. The concentrations of CdTe nanocrystals (5.0×10^{-7} M) and metal particles (2.2×10^{-7} M) were the same for all the samples in solution

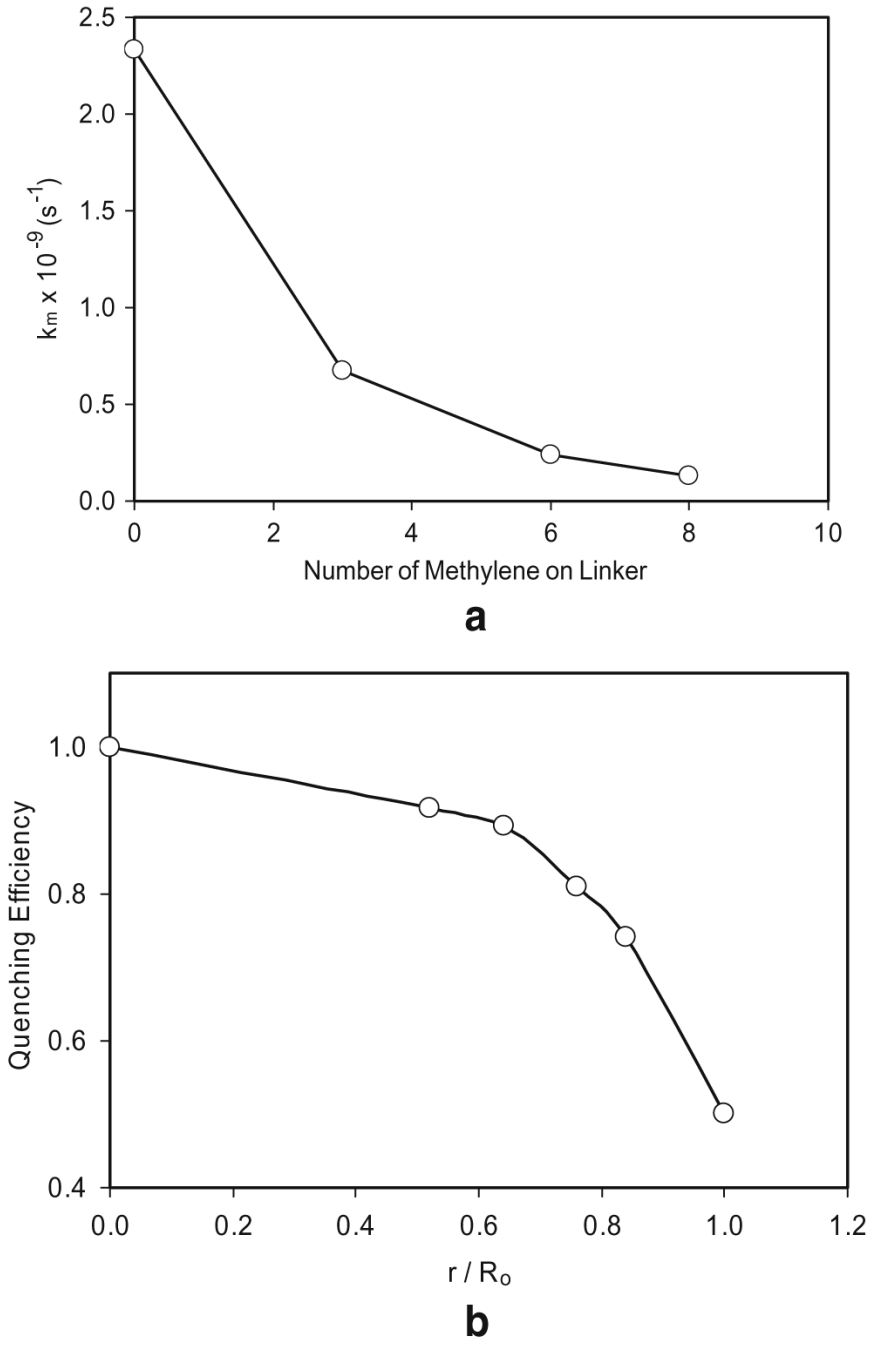

Fig. 6.

a Effect of spacer length between CdTe and gold nanoparticles on the rate fluorescence quenching (k_m) and **b** quenching efficiency. R_o is the Förster distance

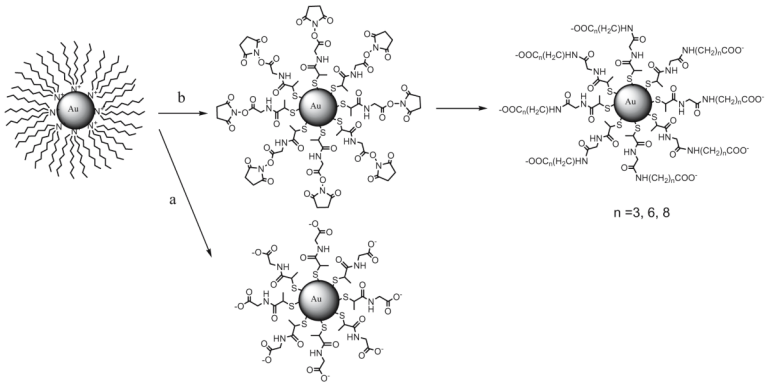

Scheme 1.

Schematic representation describing the preparation of gold nanoparticles protected with varied ligand-chain length. Tiopronin (shortest ligand used in this study)- protected nanoparticles were obtained as shown in route *a*, where the tetraoctylammonium ligands were directly displaced with tiopronin. Longer ligand-protected nanoparticles were prepared in a two-step procedure as shown in route *b*. At first, tetraoctylammonium ligands are displaced with active ester-terminated ligands and subsequent condensation with the *γ*-aminoalkyl carboxylic acid with varying methylene carbons from 3 to 8

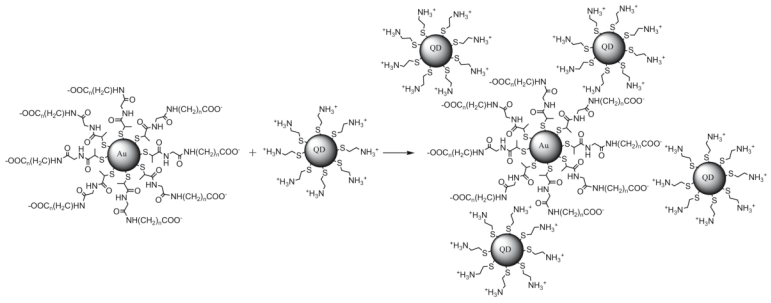

Scheme 2.
Schematic representation of electrostatic interactions in the complexes of negatively charged gold nanoparticles and positively charged CdTe nanocrystals in aqueous solution at pH 5.0

Table 1

Lifetime data obtained using the biexponential model for the CdTe nanocrystals bound with or without the metal particles

Samples	τ_i (ns)	α_i	$\langle\tau\rangle$ (ns)	χ_R^2
CdTe nanocrystal in water	1.70	0.647	21.69	1.13
	24.25	0.353		
Qdot-Au complexes methylene number				
0	2.23	0.764	12.19	1.29
	16.53	0.236		
3	2.44	0.695	14.21	1.18
	17.88	0.305		
6	3.22	0.632	15.11	1.50
	18.64	0.368		
8	2.86	0.664	16.59	1.09
	20.40	0.336		